Brownian dynamics simulations of single-stranded DNA hairpins

ARTICLE *in* THE JOURNAL OF CHEMICAL PHYSICS · APRIL 2009

Impact Factor: 2.95 · DOI: 10.1063/1.3078795 · Source: PubMed

2 AUTHORS, INCLUDING:

Kevin Dorfman
University of Minnesota Twin Cities
140 PUBLICATIONS **1,648** CITATIONS

SEE PROFILE

Brownian dynamics simulations of single-stranded DNA hairpins

Martin Kenward[a] and Kevin D. Dorfman[b]
Department of Chemical Engineering and Materials Science, University of Minnesota–Twin Cities, 421 Washington Avenue SE, Minneapolis, Minnesota 55455, USA

(Received 28 January 2008; accepted 16 January 2009; published online 3 March 2009)

We present a Brownian dynamics model which we use to study the kinetics and thermodynamics of single-stranded DNA hairpins, gaining insights into the role of stem mismatches and the kinetics rates underlying the melting transition. The model is a base-backbone type in which the DNA bases and sugar-phosphate backbone are represented as single units (beads) in the context of the Brownian dynamics simulations. We employ a minimal number of bead-bead interactions, leading to a simple computational scheme. To demonstrate the veracity of our model for DNA hairpins, we show that the model correctly captures the effects of base stacking, hydrogen bonding, and temperature on both the thermodynamics and the kinetics of hairpin formation and melting. When cast in dimensionless form, the thermodynamic results obtained from the present model compare favorably with default predictions of the *m*-fold server, although the present model is not sufficiently robust to provide dimensional results. The kinetic data at low temperatures indicate frequent but short-lived opening events, consistent with the measured chain end-to-end probability distribution. The model is also used to study the effect of base mismatches in the stem of the hairpin. With the parameters used here, the model overpredicts the relative shift in the melting temperature due to mismatches. The melting transition can be primarily attributed to a rapid increase in the hairpin opening rate rather than an equivalent decrease in the closing rate, in agreement with single-molecule experimental data. © *2009 American Institute of Physics*. [DOI: 10.1063/1.3078795]

I. INTRODUCTION

The structure and dynamics of single-stranded DNA (ssDNA) hairpins serve crucial roles in numerous biological functions.[1–3] This fact has been highlighted by recent single-molecule experiments that have provided unprecedented access into the kinetics[4] and energy landscape[1,2] of DNA hairpins at the macromolecular scale. Similar experiments have also provided new insights into the role of nucleic acid hairpins on essential biological functions.[3]

The structure and dynamics of ssDNA also play a key role in microfluidic and biosensing devices.[4–6] For example, experiments using ssDNA labeled with gold quenched fluorophores tethered to gold surfaces clearly illustrate the utility of ssDNA hairpins for sequence specific recognition,[6] including the ability to detect single-base mismatches.[5] Molecular beacon technologies, which rely on hybridization of ssDNA hairpins to double-stranded DNA (dsDNA), are also an important tool in single-stranded oligonucleotide recognition.[7] In these systems, ssDNA with fluorophore-quencher tags on opposite ends of the molecule are designed such that they form a (quenched) closed hairpin in the absence of target DNA. The target DNA's sequence is complementary to the sequence of the hairpin loop. When target DNA is introduced, the hairpin is broken and the fluorophore quencher are separated, thus providing a spectrofluorometric method to identify (in a sequence specific manner) the presence or absence of the target ssDNA strands.[7] Devices for single strand sequence recognition must meet stringent requirements (extreme sensitivity, high signal to noise ratios, and robust reusability) if they are to be used, for example, as pathogen detection systems.[8]

The ubiquity of single-stranded oligonucleotides, in particular, applications in biological settings, provides impetus to understand the effects of sequence specificity, solvent quality, temperature effects, and other parameters on the physical properties of hairpins. Theoretical tools (such as simulation methods) enhance the understanding of the molecular-scale origin of experimental results and provide additional insight in the behavior of molecules in these systems. Such tools not only benefit existing technologies but also aid in the development of emerging ones.[9]

To date, thermodynamic minimization is the most widely used method for modeling ssDNA. For example, one can readily determine a potential oligonucleotide's secondary structure using methods such as those implemented in the *m*-fold server.[10] Such work is aided by the large body of literature existing on the thermodynamic properties of both ssDNA and dsDNA.[9] However, purely thermodynamic approaches typically aim to find a heuristic minimum energy for the secondary structure, which yields little information concerning the resulting three dimensional (or tertiary) structure and, by definition, no information about the ssDNA dynamics. Indeed, methods such as free energy minimization often only provide information on the ground state (global free energy minima) of the molecules. In many cases, this does not necessarily represent the true equilibrium structure and ignores important contributions from conformational

[a]Electronic mail: mkenward@cems.umn.edu.
[b]Author to whom correspondence should be addressed. Electronic mail: dorfman@umn.edu.

fluctuations. Moreover, standard thermodynamic minimization methods[9] often neglect important contributions arising from tertiary structural properties.[9] For example, it is thought that RNA's three dimensional structure contributes to the fast folding into its native state, an effect that cannot be captured by extant energy minimization routines.[10–12]

Coarse-grained models have played an increasingly important role in understanding DNA dynamics.[13–16] In particular, dynamic simulation methods (especially ones which implement a coarse graining scheme) provide a practical alternative to thermodynamic approaches, and are becoming an increasingly important tool for studying the dynamics of biological molecules.[17–25] However, the level of detail (length and time scales) that can be feasibly included in a model is restricted by the time scales, spatial resolution of the model, and the availability of computational resources. As an example, the binding-unbinding of ssDNA hairpin loops occurs on the order of microseconds, which is beyond the scope of typical atomistic molecular dynamics simulations that probe nano- and picosecond time scales. While it is possible to reach microsecond time scales in atomistic-level simulations by using massively parallel simulations,[26] such resources are generally not available to the community at large. Therefore, at least with the present computational resources, it is necessary to coarse grain the system in order to systematically examine phenomena occurring on longer time scales.

Coarse-grained simulations appear in numerous incarnations, including Monte Carlo methods, Brownian dynamics (BD), molecular dynamics, and lattice Boltzmann simulations.[17–25] Although these methods entail a sacrifice in spatial resolution, many long-time phenomena (such as hairpin opening and closing) do not require such exquisite detail. Indeed, much of the relevant atomistic-level behavior occurs over very small time scales and could, in principle, be incorporated into a coarse-grained model through an appropriate multiscale approach. Several two bead per nucleotide models have appeared in literature,[19,21,27,28] and our model is similar in spirit to that of Schatz *et al.*[20] and Buyukdagli *et al.*[27] Our model does differ in several important respects from the latter references: we combine aspects from several models including an explicit stacking matrix, anharmonic bonding potentials, and other simplified potentials in our implementation (see the detailed model description which follows).

In this article, we present a BD simulation method for studying ssDNA. We posit that our base-backbone bead model[21] incorporates the minimal number of physical parameters required to capture the salient features of ssDNA self-interactions. To illustrate this point, we will present data on the thermodynamics and kinetics of hairpin loops consisting of ssDNA with complementary end sequences, as depicted schematically in Fig. 1. These hairpins undergo a wide variety of conformational changes, some of which can be associated with opening and closing events. The end complementarity causes hydrogen bond formation and effectively binds together the ends of the ssDNA. The binding and/or unbinding (opening and closing) are controlled by hydrogen bonding, stacking, backbone stiffness, temperature, and degree of complementarity (or lack thereof). These modulating factors give rise to a rich ssDNA conformational phase space.[11] While our focus here concerns ssDNA hairpins, the model is rather general and can be applied in the examination of ssDNA in a variety of other scenarios.

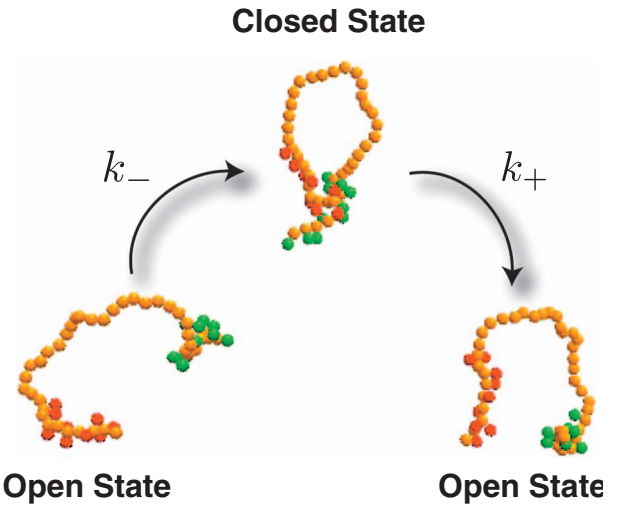

FIG. 1. (Color) Schematic figure of ssDNA hairpin transitions from open-to-closed and closed-to-open states. The ends of the ssDNA are complementary and hydrogen bond to one another. As indicated in Fig. 1, each nucleotide consists of a backbone bead connected to a base bead. In the above figure, all of the backbone beads are indicated, while only the complementary base beads at the ends of the hairpin are shown. The transitions between the states depend on temperature, degree of complementarity, backbone stiffness, stacking, and hydrogen bonding. The corresponding opening and closing rates of the hairpin are given by k_+ and k_-, respectively.

The goals of this paper are twofold: (i) We will demonstrate that the model described in Sec. II, which is simpler than other models appearing in the literature, contains sufficient physics to accurately capture the pertinent thermodynamic and kinetic properties of hairpins. To accomplish this aim, we present in Sec. III melting curves and kinetic data for the model hairpins, $A_{10}G_{20}T_{10}$ and $A_6G_8T_6$, as a function of the system parameters. (ii) We will use our model in Sec. IV to study how the melting curves and open-closed kinetics for the hairpins $A_{10}G_{20}T_{10}$ and $A_6G_8T_6$ change as the end bases are mutated to G. The latter problem has not received attention in the literature, and serves as a test bed for the versatility of our approach.

II. BROWNIAN DYNAMICS MODEL FOR ssDNA

We utilize a standard BD algorithm, as described elsewhere.[17,23] Our particular model for the ssDNA (in the context of the BD method) is effectively a base-backbone model.[21] The system is written in reduced units with a reduced temperature T. The bases A, T, C, and G are represented as single beads which are connected to backbone atoms, as schematically depicted in Fig. 2. Contiguous backbone atoms are connected to one another; a ssDNA molecule is thus comprised of multiple base-backbone units. The identity of each base is encapsulated in the particular form for the potentials quantifying the base-base, base-backbone, and backbone-backbone interactions. In addition, the molecules obey excluded volume (i.e., the Pauli principle) and each unit must be appropriately bonded to other units.

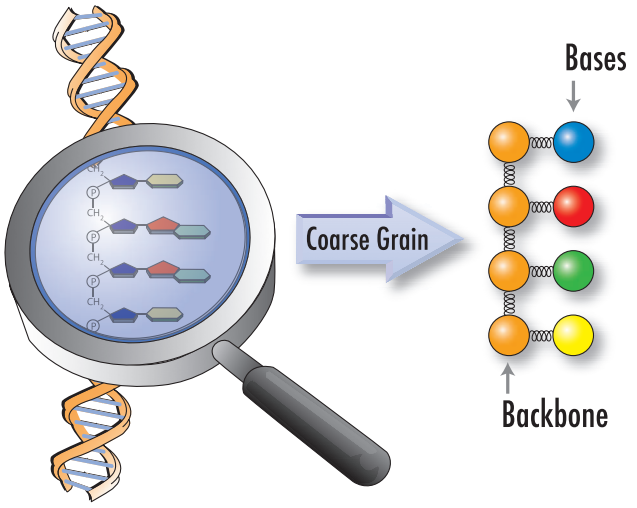

FIG. 2. (Color) Schematic depiction of BD coarse graining scheme. These *effective* bases and backbone units form the ssDNA chain and are represented as single beads in the context of the BD simulations. Appropriately chosen potentials provide the interactions between the units on the DNA.

A. Interaction potentials

Excluded volume interactions (which occur between all species) are modeled using the truncated pairwise Lennard-Jones potential,

$$U_{\mathrm{LJ}}(r_{ij}) = \begin{cases} 4\epsilon\left[\left(\frac{\sigma}{r_{ij}}\right)^{12} - \left(\frac{\sigma}{r_{ij}}\right)^{6}\right] + \epsilon, & r_{ij} \leqslant r_c \\ 0, & r_{ij} \geqslant r_c, \end{cases} \tag{1}$$

where τ_{ij} is the distance between beads i and j and r_c is the minimum in the Lennard-Jones potential. The parameters ϵ and σ represent the base units for energy and length in the model; subsequent potentials and distances will be defined in terms of these base units.

The connectivity between the various species (base/backbone and backbone/backbone) is achieved with the use of a modified harmonic potential, which ensures finite extensibility.[29] This potential is given by the so-called finitely extensible nonlinear elastic potential,

$$U_{\mathrm{bond}}(r_{ij}) = -\frac{\kappa}{2}R_0^2 \ln\left[1 - \left(\frac{r_{ij}}{R_0}\right)^2\right]. \tag{2}$$

In Eq. (2), κ is the effective strength of the potential and R_0 is the cutoff of the potential. We use the values $\kappa = 30.0\epsilon/\sigma^2$ and $R_0 = 1.5\sigma$, independent of the type of bond.[29] Although the chemistry of the bonds connecting backbone-backbone and base-backbone is rather different, the choice of parameters here yield fairly stiff springs. At our level of coarse graining, stiff springs are sufficient to describe both bonds, as we are mostly concerned about the connectivity between different parts of the backbone, rather than a detailed examination of the particular internal modes of the molecules. All beads are prescribed the same unit mass in the simulations. The molecules are initiated as linear molecules with unit spacing between the beads.

To provide some additional stiffness to the backbone of the molecule, we utilize a bending potential

$$U_b(\theta) = \frac{u_b}{2}(\cos\theta + \cos\theta_0)^2 \tag{3}$$

applied only to contiguous backbone beads. The parameter θ_0 is the desired bending angle along the backbone, and u_b is a tunable parameter dictating the effective stiffness of the molecule ($u_b = 0$ implies a freely jointed chain, while $u_b \gg 0$ implies a stiff molecule). In all cases we use $\theta_0 = 0$ and $u_b = 18\epsilon$. These parameters give a persistence length for the molecule on the order of a few beads.

The other key interactions governing ssDNA and dsDNA (and indeed RNA) structure and dynamics are base stacking (which is often simply referred to as stacking) and hydrogen bonding.[9] Stacking occurs as a result of a favorable free energy associated with bases effectively lying on top of each other.[9] This is a result of several contributions, including steric interactions.[9] Stacking is in large part responsible for the stabilization of the double helical structure of dsDNA (Ref. 9) and occurs between *contiguous* bases. For both interactions, we use the potential

$$U_k(r_{ij}) = -\epsilon u_k \delta_{ij}^k \left\{\exp\left[20\left(\frac{r_{ij}}{\sigma} - \Gamma_s\right) + 1\right]\right\}^{-1}, \tag{4}$$

where k=stack or k=hbond, depending on which energy U_k quantifies. The parameter u_k is gives the overall strength of the stacking/hydrogen bonding interaction.[21] The individual δ_{ij}^k's give *identity* of each base and describe how a base of type i and j interact with one another through stacking/hydrogen bonding. The parameter $\Gamma_s = 1.5$ for both stacking and hydrogen bonding. The δ_{ij}^k's in Eq. (4) provide the base pair specificity. For simplicity we define a stacking matrix

$$\Delta_{ij}^{\mathrm{stack}} = \begin{bmatrix} \delta_{\mathrm{AA}}^{\mathrm{stack}} & \delta_{\mathrm{AT}}^{\mathrm{stack}} & \delta_{\mathrm{AC}}^{\mathrm{stack}} & \delta_{\mathrm{AG}}^{\mathrm{stack}} \\ \delta_{\mathrm{TA}}^{\mathrm{stack}} & \delta_{\mathrm{TT}}^{\mathrm{stack}} & \delta_{\mathrm{TC}}^{\mathrm{stack}} & \delta_{\mathrm{TG}}^{\mathrm{stack}} \\ \delta_{\mathrm{CA}}^{\mathrm{stack}} & \delta_{\mathrm{CT}}^{\mathrm{stack}} & \delta_{\mathrm{CC}}^{\mathrm{stack}} & \delta_{\mathrm{CG}}^{\mathrm{stack}} \\ \delta_{\mathrm{GA}}^{\mathrm{stack}} & \delta_{\mathrm{GT}}^{\mathrm{stack}} & \delta_{\mathrm{GC}}^{\mathrm{stack}} & \delta_{\mathrm{GG}}^{\mathrm{stack}} \end{bmatrix} = \frac{1}{4}\begin{bmatrix} 3 & 2 & 2 & 3 \\ 2 & 1 & 1 & 2 \\ 2 & 1 & 3 & 3 \\ 3 & 2 & 3 & 4 \end{bmatrix}, \tag{5}$$

where $\delta_{ij}^{\mathrm{stack}}$'s in Eq. (5) represent all possible base pair stacking combinations.[19] In the present version of this model we do not incorporate cross-stacking interactions.[19]

Hydrogen bonding occurs between complementary bases (AT and GC pairs) and effectively binds two complementary sequences to one another.[19] To model hydrogen bonding in our simulations we use the potential given in Eq. (4) with k=hbond. The effective hydrogen bonding is given by the antidiagonal matrix

$$\Delta_{ij}^{\mathrm{hbond}} = \begin{bmatrix} 0 & 0 & 0 & \delta_{\mathrm{AT}}^{\mathrm{hbond}} \\ 0 & 0 & \delta_{\mathrm{CG}}^{\mathrm{hbond}} & 0 \\ 0 & \delta_{\mathrm{GC}}^{\mathrm{hbond}} & 0 & 0 \\ \delta_{\mathrm{TA}}^{\mathrm{hbond}} & 0 & 0 & 0 \end{bmatrix}. \tag{6}$$

In other words, only AT and GC base beads interact by hydrogen bonding with one another. We exclude hydrogen

bonding interactions between contiguous base beads, even if they are an AT or GC pair. Naturally, the hydrogen bonding and stacking energies do not apply to backbone beads. The individual $\delta_{ij}^{\text{hbond}}$'s provide the base pair specific interaction between complementary sequences on the ssDNA. In this model we have chosen $\delta_{\text{CG}}^{\text{hbond}}=\delta_{\text{GC}}^{\text{hbond}}=1$ and $\delta_{\text{TA}}^{\text{hbond}}=\delta_{\text{AT}}^{\text{hbond}}=2/3$ reflecting the fact that GC and AT pairs participate in three and two hydrogen bonds respectively.

We also exclude hydrogen bonding interactions between base i and base $j=i\pm2$ to prevent the formation of three-membered rings. This choice is motivated by the heuristic criteria one observes in the m-fold server,[10] where such rings are normally excluded when one employs moderate values of the ionic strength. In the present model, the isotropy of the hydrogen bonding interactions can, in principle, lead to three-member rings through an unrealistic twisting of the backbone chain and interactions through the phosphate backbone or along oblique angles that should not, in reality, lead to significant hydrogen bonding interactions. That being said, the test chains that will be studied here cannot form such rings and the latter restriction becomes superfluous.

B. Time integration

Given the positions $\mathbf{r}_i(t)$ of all of the N beads in the system, the position dependent energy of bead i is given by the sum

$$U_i(\mathbf{r}_i(t))=U_{\text{LJ}}+U_{\text{bond}}+U_b+U_{\text{stack}}+U_{\text{hbond}}, \tag{7}$$

where the potentials on the right-hand side refer to the relevant values for bead i. As described in Sec. II A, the parameters appearing in these potentials are completely defined in terms of ϵ and σ, except for the (dimensionless) strengths of stacking, u_{stack}, and hydrogen bonding, u_{hbond}. The latter parameters will be specified in the context of the particular simulations detailed below.

The equations of motion governing the time-dependent positions $\mathbf{r}_i(t)$ of each bead in the simulation are given by the Langevin equation

$$\xi\frac{d\mathbf{r}_i(t)}{dt}=-\nabla_r U(\mathbf{r}_i(t))+\mathbf{f}_i(t), \tag{8}$$

where ξ is the friction coefficient of each bead. We assume that the friction coefficients of base and backbone beads are identical. The stochastic forces, $\mathbf{f}_i(t)$, satisfy the fluctuation dissipation theorem:

$$\begin{aligned}&\langle\mathbf{f}_i(t)\rangle=0,\\&\langle\mathbf{f}_i(t)\cdot\mathbf{f}_j(t')\rangle=6\xi k_BT\delta(t-t')\delta_{ij},\end{aligned} \tag{9}$$

where k_BT is the Boltzmann factor and δ_{ij} is the Kronecker delta function.

The solution of Eq. (8) is obtained by first rendering it dimensionless with the length scale σ and the time scale $\xi\sigma^2/\epsilon$, which implies a dimensionless temperature k_BT/ϵ. Subsequently, we will use the symbol T to denote the dimensionless temperature. The equations are then integrated numerically using the velocity Verlet algorithm.[30] Typical time steps in the integration method are on the order of $\delta t=0.01$. At the start of the simulation, the molecules are initialized as linear chains. To ensure relaxation from this initial state, the simulations are carried for 1×10^6 BD time steps to erase memory of the initial configuration. The molecules are then simulated for approximately 1×10^8 BD time steps. The total simulation times allow sufficiently large numbers of opening and closing events to allow reliable measures of average opening and closing times. Independent runs with different initial conditions were performed to ensure robustness with respect to the starting conformations of the molecules.

C. Limitations of the model

It is our opinion that the latter model includes the minimum amount of microscale physics necessary to capture the salient properties of DNA hairpins. Explicitly, the combination of excluded volume, stacking, and hydrogen bonding interactions are the key elements necessary to model the ssDNA of our simulations. That being said, a few remarks are also in order about the limitations of the model. First, we have assumed that the interaction potentials are isotropic. While the interactions should have some degree of anisotropy (for example, hydrogen bonding), isotropic potentials provide a sufficient degree of accuracy at our level of coarse graining, provided we exclude hydrogen bonding interactions that can form three-member rings. Explicitly, the various backbone potentials, such as the excluded volume, and the short-ranged nature of the stacking and hydrogen bonding potentials prevent aphysical scenarios such as hydrogen bonding of bases through the backbone. Moreover, isotropic potentials side step the need to introduce additional *ad hoc* parameters in order to characterize the nature of the anisotropy. Second, we have not included hydrodynamic[31,32] or explicit electrostatic interactions in the current incarnation of this model. Although electrostatic interactions (and thus the effects of salt) are important in modeling biological macromolecules, they are prohibitively expensive (in the computational sense). As we are interested in a simulation model that is capable of accessing long time scales, the explicit salt molecules are neglected. This is fairly standard approach used in coarse-grained modeling.[15,17,19,27] Thus, coarse-grained models can capture (in a qualitative way) the screening due to Debye–Huckel theory by making the interaction potentials a function of ionic strength. However, a coarse-grained model cannot capture coordination caused by multivalent ions. If such coordination is important, an atomistically detailed simulation scheme is required. More detailed models which include explicit ions and electrostatics are possible; however, they generally come at hefty computational cost.[33,34] It is also worthy to note that this particular model is also unable to distinguish between the 5′ and 3′ ends of the ssDNA and the ssDNA and the concomitant handedness of dsDNA. Chirality can be enforced in several ways.[17,35] While chirality is essential for quantifying many biological processes, such as protein binding into the minor or major groove, it is not a critical component in the hairpin kinetics problem studied here.

III. MODEL VALIDATION

As noted at the outset, our first aim is to demonstrate that our model captures the salient thermodynamic properties of ssDNA hairpins. In doing so, we demonstrate that although the model does not include all of the features of previous models,[17] it constitutes an attractive compromise between spatial detail and computational time. To accomplish this goal, we first study the thermodynamics of the test chain sequences $A_{10}G_{20}T_{10}$ and $A_6G_8T_6$, examining the melting of these ssDNA hairpins as a function of reduced temperature, T, the hydrogen bonding energy, u_{hbond}, and the stacking energy, u_{stack}. To simplify our investigation we set $u_{\mathrm{stack}}=u_{\mathrm{hbond}}=u_{\mathrm{shb}}$, thus reducing the problem to a single energy parameter. In addition, we also investigate the kinetics of both hairpins, thereby illustrating the ability to obtain dynamical information and insights into the model predictions of the dependence of the melting temperature on the size of the hairpin stem.

A. Thermodynamics

Our metric to determine the state of the ssDNA (open or closed) is defined in terms of the number of complementary interactions between the bases at the ends of the molecules, n_{o}. In other words, if two bases are within a distance where the hydrogen bonding potential is effectively nonzero (since it decays very quickly as a function of distance) the two bases are considered to be participating in complementary interactions. We define the total number of bases in a molecule to be N_{base}, the number of complementary end base pairs to be N_c, and the number of noncomplementary bases to be N_{nc}, such that $N_{\mathrm{base}}=2N_c,+N_{\mathrm{nc}}$. If $n_{\mathrm{o}}<N_c$ the ssDNA is considered to be in the *open* state and vice versa for the *closed* state. By monitoring n_{o} as a function of time, we can access the fraction of open and closed states. The fraction of melted states, ϕ_m, is the total number of open states divided by the total number of observed states, n_{tot}, while the fraction of closed states is simply $\phi_c=1-\phi_m$.

For our test chain sequence ($A_{10}G_{20}T_{10}$), we first (and for illustrative purposes) examined the melting of the ssDNA hairpin as a function of reduced temperature T for the fixed bonding energy $u_{\mathrm{shb}}=1.0$. The associated melting curves (i.e., ϕ_m versus T), shown in Fig. 3, agree with the qualitative thermodynamic behavior of hairpins. At very low temperatures relative to the binding energy, the thermal energy of the system is simply too small to overcome the binding energy—once the hairpin closes, it cannot open. Conversely, for large T the thermal energy is much larger than the binding energy and the molecule is effectively a random coil. Some fraction of the random coil states would correspond to closed conformations by our metric, but the vast majority are open states.

The effective melting temperature, T_m, at which the molecule has an equal probability of being open or closed, can be defined in one of two ways. The first definition is the point at which the melting curve intersects a line at $\phi_m=\frac{1}{2}$. Alternatively, one can fit the melting curve with a sigmoidal distribution (as shown in Fig. 3). The peak in the derivative of this fitted curve gives the inflection point of the melting curve and thus another measure of the melting temperature.

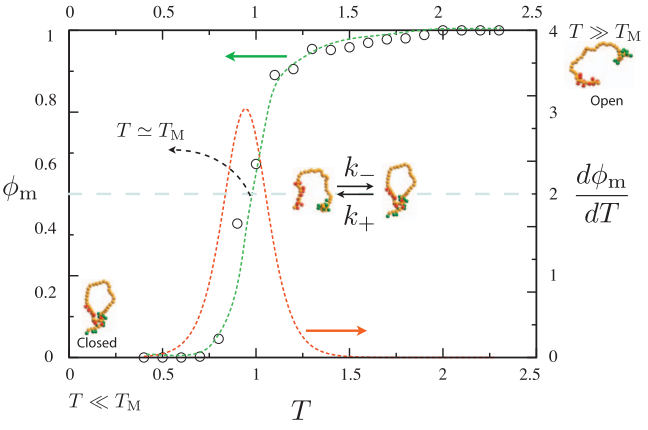

FIG. 3. (Color) Sample melting curve, ϕ_m versus temperature, for our test ssDNA sequence ($A_{10}G_{20}T_{10}$) for $u_{\mathrm{shb}}=1.0$. The melting curve ϕ_m corresponds to the open circles (overlayed dashed line is shown as a guide for the eye). The axes on the left of the figure corresponds to ϕ_m. The derivative $d\phi_m/dT$ of a fit to the melting curve using a sigmoidal distribution is also shown. The axes on the right corresponds to $d\phi_m/dT$.

In this particular example, both methods furnish a similar melting temperature, $T_m\simeq 0.95$. This figure primarily illustrates the ability of our relatively simple model to capture the characteristic melting behavior of ssDNA hairpins.

Although we have defined our metrics for the open and closed states in terms of n_{o}, the number of formed complementary pairs, it is possible to use other measures to determine whether the molecule is in an open or closed state. For example, we can monitor the evolution of the end-to-end distance, R_{e2e}, and its associated distribution, $\rho(R_{\mathrm{e2e}})$, as a function of temperature. Figure 4 shows a plot of the normalized probability distribution of the end-to-end distance for three different temperature regimes. For temperatures well below the melting temperature, the distribution $\rho(R_{\mathrm{e2e}})$ exhibits a single (relatively sharp) peak at low R_{e2e}. The end-to-end distance is measured as the distance between the end

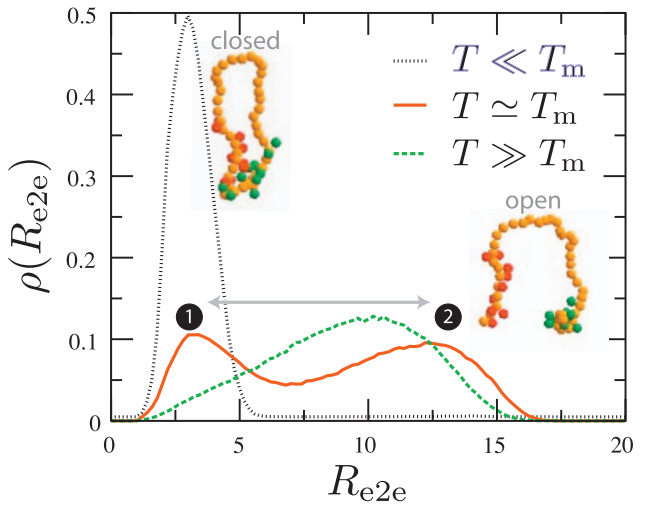

FIG. 4. (Color) Plot of the distribution of the end-to-end distance, $\rho(R_{\mathrm{e2e}})$, as a function of temperature, T, for three different regimes appearing in Fig. 3: for $T=0.5\ll T_m$ the molecules primarily populate the closed state, while for $T=1.8\gg T_m$ the molecules are predominantly in the open state and fully melted. In the region where $T=1.0\simeq T_m$, it is equiprobable to find the molecules in either the open and closed states.

sugar-phosphate backbone groups on the DNAs. The position of the peak value of R_{e2e} (for low T) is on the order of the center to center distance between the two sugar-phospate groups with two interstitial bases. This primary peak is indicative of molecules in the closed state.

With increasing T the distribution shifts toward higher $\rho(R_{e2e})$ and becomes skewed; this is followed by the appearance of a secondary peak corresponding to molecules that are in the open state. As $T \to T_m$, the primary and secondary peaks become roughly the same height (as seen in Fig. 4). Further increasing T leads to the disappearance of the primary peak and a broadening of the secondary peak, and the molecule effectively always remains in the open state with a wide distribution of end-to-end distances. At high T, the end-to-end distance, R_{e2e}, tends toward an equilibrium value. We would expect this equilibrium value to be on the order of the radius of gyration for an excluded volume chain ($R_g \sim N^\nu$ with $\nu = 3/5$).[36] Indeed we find that $R_g \sim 40^{3/5}\sigma \approx 9\sigma$, which is what we observe in Fig. 4.

Using the end-to-end distance, R_{e2e}, provides more insights into the statistical physics of melting and annealing when compared with the data based on ϕ_m. Consider the different types of "open states" for $T \ll T_m$ and $T \gg T_m$. As seen in Fig. 4, the dominant type of open state for $T \ll T_m$ has an end-to-end distance on the order of twice that of the closed state. In contrast, the end-to-end distances for the distribution of open states realized for $T \gg T_m$ are markedly larger than the characteristic distance $R_{e2e} \sim 3\sigma$ of the closed state. The characteristic sizes of open states with temperature can be understood in the context of a biased random walk of the hairpin end. When the hairpin escapes from the energy barrier imposed by base pairing, one of its free ends undergoes a random walk in the presence of a probability density sink represented by the complementary sequence located on the other end of the ssDNA. The strength of the sink is related to the temperature for a fixed value of u_{shb}. As a result, the diffusive flux toward the sink increases as the temperature decreases. At low temperatures, the excursions away from the closed state engendered by thermal energy are opposed by a gradient in probability density at the sink, leading to a narrower probability distribution $\rho(R_{e2e})$. When the temperature is large, $T \gg T_m$, the sink strength is negligible. In the absence of a probability density gradient near the sink, the hairpin end is able to explore a much wider region of the phase space.

The affinity of complementary sequences is primarily controlled by the effective strength of the hydrogen bonding between the bases, which is governed by u_{hbond}. In order to examine binding of the complementary end sequences on the molecules, we varied the parameter u_{shb} and measured the associated melting curve (ϕ_m versus T) for our test sequence, shown in Fig. 5. For the lowest value of $u_{shb} = 0.6$ (leftmost curve) the melting curve is somewhat steplike and leads to a melting temperature of $T_m \simeq 0.5$. As u_{shb} is increased the melting curve shifts toward increasing T_m. It is worth noting that the particular shapes of the melting curves depend to a small degree on the metric used to define the open and closed states.

One would expect that the melting transitions would be relatively sharp when presented on the dimensionless temperature scale in Fig. 5. Explicitly, we obtained a melting temperature of 61.7 °C for this hairpin using the m-fold server with the default values.[37] We would expect that the hairpins should melt completely before reaching the boiling point of water. Assuming that the melting temperature predicted by m-fold constitutes a realistic estimate, one would expect to reach the upper plateau of ϕ_m at a dimensionless temperature no higher than $T \simeq 1.1T_m$. This appears to be the case for the lower values of u_{shb}. In contrast, the higher values of u_{shb} spread the melting transition up to $T \simeq 1.5T_m$, which should be well above the boiling point of water.

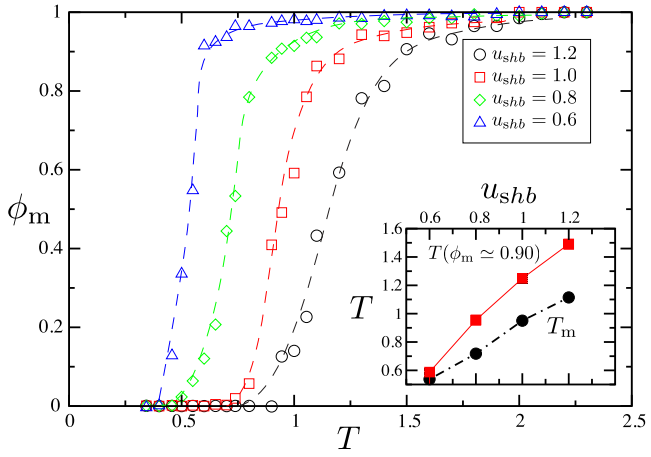

FIG. 5. (Color online) Melting curves, ϕ_m vs T, for several values of u_{shb} for the sequence appearing in Fig. 3. Inset figure shows how the melting temperature (circles) and the temperature at which $\phi_m = 0.90$ (squares) depend on the parameter u_{shb}. Qualitatively the latter temperature corresponds to the open state. The lines on the figure are shown as a guide for the eye.

The inset of Fig. 5 reveals that the melting temperature, T_m, exhibits an approximately linear dependence on the bonding energy, u_{shb}. This is to be expected—both the temperature and the bonding interactions are made dimensionless with the energy scale ϵ. However, note that the melting point does not occur at the point $T = u_{shb}$ because ten hydrogen bonds must be broken in order to melt this hairpin. We have also determined the melting temperature for the somewhat shorter sequence $A_6G_8T_6$ (see Fig. 8). The melting temperature decreases from $T_m \simeq 0.95$ for $A_{10}G_{20}T_{10}$ to $T_m \simeq 0.75$ for $A_6G_8T_6$ at a fixed value $u_{shb} = 1.0$. The ratio of these two melting temperatures, 1.25, is higher than that predicted value of 1.02 predicted by m-fold[37] for the default solution values. (The predicted temperature[37] for $A_6G_8T_6$ is 54.2 °C.) As the m-fold server thermodynamic results are based on extensive experimental data,[38] we can thus conclude that our model, with the parameters chosen here, only qualitatively captures the increase in melting temperature with the size of these hairpins.

B. Kinetics

In Sec. III A, we considered the thermodynamic properties of ssDNA hairpins. The latter could be obtained by many methods, including "static" approaches such as energy minimization. As such, the qualitative thermodynamic behavior of ssDNA hairpins are well known, and the results obtained

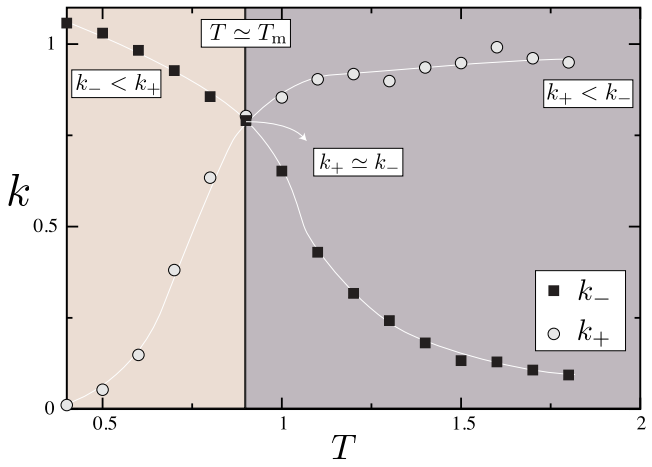

FIG. 6. (Color online) Kinetic constants for the sequence $A_{10}G_{20}T_{10}$. The constants for the opening and closing rates are given by k_+ and k_-, respectively (in inverse BD steps). The time step in the BD simulations is $\delta t = 0.01$. The kinetic constants have three different regimes: (i) the temperature is below the melting temperature $T < T_m$ ($k_- < k_+$) and the molecule is primarily in the closed state; (ii) at the melting temperature $T = T_m$ ($k_- = k_+$) and the molecules are in dynamic equilibrium between the open and closed states; and (iii) the temperature is well above $T > T_m$ ($k_- > k_+$) and the molecules are primarily in the open state. Lines on the figure are shown as a guide for the eye. The data correspond to $u_{shb} = 1$.

above validate our overall approach. In the present subsection, we proceed to investigate dynamic properties of ssDNA hairpins, namely, the open-to-closed and closed-to-open transitions. A complete understanding of these transitions, in particular, their sequence dependence, is lacking in the literature. Our ability to resolve such kinetic rates in a computationally efficient way constitutes the primary advantage of our dynamical method.

The dynamics of hairpin closing and opening are quantified by the rate constants, k_- and k_+, respectively.[39] Estimates of these constants are obtained by monitoring the distribution of dwell times with lifetimes having a duration of at least τ (where τ is defined in units of 100 BD time steps; consequently k_- and k_+ are in units of inverse BD time steps with a value of $\delta t = 0.01$). These dwell time distributions are denoted by $N_c(\tau)$ and $N_o(\tau)$ for the closed and open states, respectively, while the total number of observed closed and open states are N_c^{tot} and N_o^{tot}.

The functional form of the dwell time distributions is expected to obey an Arrhenius-like relationship as a function of τ and can be written as

$$\frac{N_{c(o)}(\tau)}{N_{c(o)}^{\text{tot}}} \equiv k_{+(-)} e^{-k_{+(-)}\tau}. \tag{10}$$

By fitting the calculated dwell time distributions [$N_c(\tau)$ and $N_o(\tau)$] from our BD simulations, we obtain estimates of k_- and k_+.

Figure 6 shows a plot of k_- and k_+ for the sequence $A_{10}G_{20}T_{10}$ as a function of temperature. The melting temperature is $T_m \simeq 0.9$. These kinetic rates are not only consistent with the qualitative behavior obtained in Sec. III but also provide insights into the time scales relevant to the structural transitions. Below the melting temperature ($T < T_m$), the opening rate is much lower than the closing rate ($k_- \ll k_+$). With increasing temperature k_- decreases while k_+ increases. At the melting temperature, $T = T_m$ and the kinetic constants are equal, $k_- = k_+$. At this point it is equiprobable to find the molecules in either the closed or open states. At larger T the opening rate continues to increase, whereas the closing rate decreases and tends toward zero, i.e., $k_- \to 0$. Remarkably, the closing rate is not completely quenched since thermal motion can bring the end segments into close proximity, even if the hydrogen bonding is not strong. When $T \gg T_m$ we have $k_- \gg k_+$ and the molecules are primarily in the open state. Closing events are then short lived and infrequent.

It is illustrative to consider in more detail the kinetics below the melting point. From a thermodynamic perspective such as the one adopted in Fig. 3, we would classify these chains as closed. In an experiment, such thermodynamic data could be obtained from a UV adsorption or fluorescence resonance energy transfer (FRET) experiment. However, multiple kinetic explanations are consistent with a standard melting curve based on the fraction of open hairpins, ϕ_m. For example, the first-order transition in Fig. 3 could correspond to closing and opening kinetics that reach plateaus well below the melting point, and then rapidly transfer to new plateau values over the transition between $\phi_m \sim 0$ and $\phi_m \sim 1$. However, this is not the case from our study. The closed state does not correspond to a complete quenching of the opening rate, and the opening rate increases quite quickly with temperature below the melting point in agreement with experiments.[4] Thus, although the hairpin is closed on average, our kinetic analysis indicates that there should be many short-lived excursions between the open and closed states at low temperatures. The latter dynamical observation is consistent with the end-to-end distribution presented in Fig. 4 for $T \ll T_m$. Indeed, if the opening rate was completely quenched, the distribution $\rho(R_{e2e})$ would be much more sharply peaked.

It is also worth noting that in the particular case we show, the final temperature is about four times that of the melting temperature T_m, which is well beyond the normal operational temperature in experimental systems.[9,38] Based on the m-fold predicted melting temperature, we would expect the boiling point of water in this figure to be $T \simeq 1.03$.

IV. MISMATCHED HAIRPIN STEMS

Having established the validity of our method and its ability to capture kinetic data, we now proceed to study the thermodynamics and kinetics of hairpins with mismatches in their stems. While the effect of bonding between one side of the stem and a region of the loop has been studied at a highly coarse-grained level by Monte Carlo methods,[25] it does not appear that mismatches in the stem have been addressed in the literature. Qualitatively, in the limiting case of a strand which has no complementary sequence, we expect no hairpin formation. As we increase the degree of complementarity of the end sections of the ssDNA hairpins, we increase the likelihood that the ends will bind to one another. As a result, not only should the binding/unbinding of the hairpins depend on

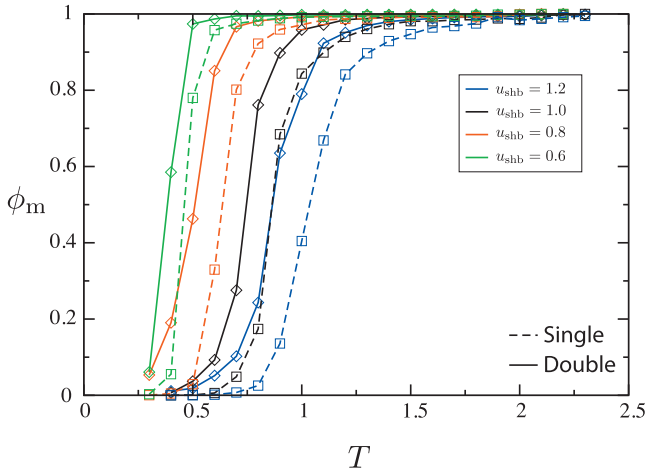

FIG. 7. (Color) Melting curves, ϕ_m vs temperature, for two different partially mismatched end sequences and several values of the parameter u_{shb}. The sequences are $G_2A_8G_{20}T_8G_2$ for the double-mismatched sequence (solid lines) and $G_1A_9G_{20}T_9G_1$ for the single-mismatched end sequence (dashed lines).

the effective value of u_{shb} but it should be sequence specific. Higher complementarity should translate into stronger binding interactions.

In order to examine the change in hairpin formation resulting from mismatches, we started with the sequence $A_{10}G_{20}T_{10}$, whose kinetic data appear in Fig. 6, and proceeded to mutate the ends of the stem to make a single-mismatched hairpin, $G_1A_9G_{20}T_9G_1$, and a double-mismatched hairpin, $G_2A_8G_{20}T_8G_2$, that have the same molecular weight and loop size as the perfectly matched hairpin. Figure 7 shows a plot of the melting curves for these two different sequences for four different values of u_{shb}. For each value of u_{shb} the single-mismatched molecule has a higher melting temperature and the melting curve is shifted to the right relative to the double-mismatched case. Mismatches have the effect of decreasing the melting temperature of the molecules as they lower the energy barrier for the chain to melt. This effect plays an important role in binding/unbinding transitions, and the method proposed here could be used to address a number of unanswered questions related to, for example, mismatch melting and PCR primer design protocols.[8]

Table I presents the change in the melting temperature due to mismatches at four different values of the bonding energy u_{shb}. In melting experiments for linear probes,[40] one observes a characteristic shift in the melting temperature from $T_m^{mismatch} \simeq 40\ ^\circ C$ for a single mismatch to $T_m^{perfect} \simeq 50\ ^\circ C$ for the complementary chain. Although the latter experiment does not correspond exactly to the hairpin problem studied here, it provides a useful estimate of the ratio $T_m^{perfect}/T_m^{mismatch} \simeq 1.03$. We have also inputted the two sequences appearing in Fig. 7 into *m*-fold using the default parameters[37] and obtained a melting temperature of 59.4 °C for the single mismatch and 56.5 °C for the double mismatch. With the *m*-fold melting temperature of 61.7 °C for the perfect match, this corresponds to the temperature ratios in Table I. Although our measures of the relative shift in melting temperature are higher than those presented by

TABLE I. Comparison of the ratio of melting temperatures, $T_m^{perfect}/T_m^{mismatch}$, between the *m*-fold server (Ref. 37) and the present model for four different values of u_{shb} for the two hairpins, $A_6G_8T_6$ and $A_{10}G_{20}T_{10}$. The upper bounds for the errors on the ratio of melting temperatures are $\sigma = \pm 0.05$ for the $A_6G_8T_6$ sequence and $\sigma = \pm 0.06$ for the $A_{10}G_{20}T_{10}$ sequence.

	$A_6G_8T_6$	u_{shb}			
Mismatch	*m*-fold	0.6	0.8	1.0	1.2
Single	1.02	1.04	1.07	1.09	1.07
Double	1.05	1.13	1.15	1.19	1.23
	$A_{10}G_{20}T_{10}$	u_{shb}			
Mismatch	*m*-fold	0.6	0.8	1.0	1.2
Single	1.01	1.11	1.12	1.15	1.15
Double	1.02	1.25	1.30	1.34	1.38

Libchaber *et al.*[40] and those obtained from *m*-fold server predictions, they are certainly within a reasonable range. The fine-tuning of these relative temperature shifts can be achieved by varying the parameters in our BD model. A possible approach to fine-tuning the parameters is described at the conclusion of this paper.

In addition to the above sequence, Fig. 8 contains a series of melting curves for the sequence $A_6G_8T_6$ and the single and doubly mismatched sequences $G_1A_5G_8T_5G_1$ and $G_2A_4G_8T_4G_2$, respectively. Table I also shows the predicted change in melting temperatures from the simulations along with default *m*-fold calculations. As for the large hairpin, the melting curves follow the trend that there is a decrease in melting temperature for decreasing u_{shb} and have a characteristic sigmoidal shape. The ratios of the melting temperatures are also still higher than those predicted by *m*-fold calculations.

We also investigated the effects of end mismatches on the rate constants of opening and closing events for the sequences shown in Fig. 9. Mismatches (either internal or at the ends of the molecules) can significantly alter hairpin

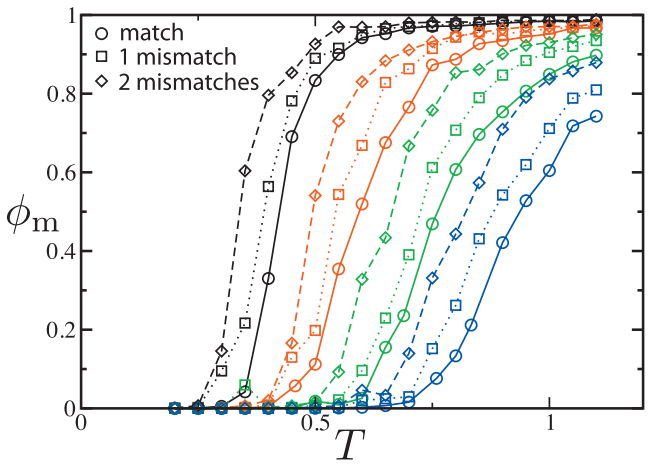

FIG. 8. (Color) Melting curves, ϕ_m vs temperature, for two different partially mismatched end sequences and several values of the parameter u_{shb}. The sequences are $A_6G_8T_6$ fully matched sequence (solid lines) $G_1A_5G_8T_5G_1$ for the single-mismatched sequence (dotted lines) and $G_2A_4G_8T_4G_2$ for the double-mismatched end sequence (dashed lines).

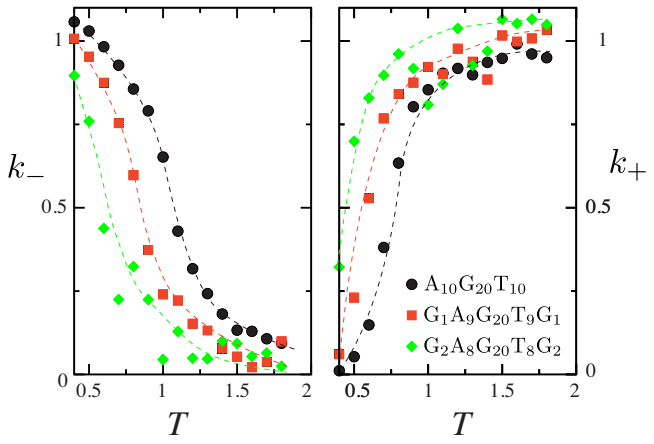

FIG. 9. (Color online) Kinetic constants for the sequence $A_{10}G_{20}T_{10}$ and the single and double end mismatched sequences $G_1A_9G_{20}T_9G_1$ and $G_2A_8G_{20}T_8G_2$. The left and right panels of the figure show the closing and opening rates, k_- and k_+, as a function of reduced temperature. End mismatches decrease the closing rate and increase the opening rate, as a result of the reduced affinity of the complementary sections of the molecules. Lines are shown as guides for the eye. The data correspond to $u_{\mathrm{shb}}=1$.

dynamics.[1] Figure 9 depicts the opening and closing rates (shown on the left and right panels, respectively) for the sequence $A_{10}G_{20}T_{10}$ and the same sequence with single- and double-mismatched ends, $G_1A_9G_{20}T_9G_1$ and $G_2A_8G_{20}T_8G_2$. Inducing a higher degree of mismatch at the ends decreases the closing rate, k_-, and increases the opening rate, k_+, while the overall shapes of these curves remain similar as the number of mismatches increases. The spacing between the curves provides a tell-tale signature of the start of the transition between the closed and open states. For example, consider the change in the gap between the curves for the closing rate, k_-, as the temperature increases. At very low temperatures, the gap between the single and double mismatches quickly increases as the double mismatch begins to melt (and hence adopts a slower closing rate). In contrast, the gap between the single-mismatch closing rate and the perfect match closing rate remains relatively stable until a higher temperature, at which point the single-mismatch hairpin begins to melt.

Based on the slopes of the kinetic curves, the closed-to-open transition can be attributed more to an increase in the opening rate than a decrease in the closing rate. Indeed, as we move from a very low temperature to near the melting point, the opening rate increases from nearly zero to close to 80% of its maximum value, while the closing rate has only decreased by a factor of on the order of $1/2$. This behavior is observed for all of the hairpins, independent of the degree of mismatch. The latter behavior is consistent with fluorescence correlation spectroscopy results for DNA hairpins,[4] which clearly indicate that the opening rate has a much stronger temperature dependence than the closing rate. However, the latter experiments show a minimal dependence of the closing rate with temperature. While this contrasts with our results, the temperature range of the experiments is quite limited compared to what is presented here. The kinetic rates in the latter experiments[4] have also been called into question recently.[41]

As the temperature increases past the melting point, the hydrogen bonding interactions become weak compared to thermal energy. As a result, the mismatches play an ever diminishing role in determining the opening and closing rates and the various curves begin to converge. The scatter in the data also makes it clear that it is quite difficult to obtain an accurate measure of the kinetic rates at high temperatures. The main source of the scatter are random events that bring the chain ends into proximity, which are counted as closing events by the metrics employed here.

Although we provided only a preliminary examination of the effects of end mismatches on the opening and closing rates, this is a rather broad topic and a robust and systematic study of these effects is still lacking in the current literature. Experimental methods[1,4,40] are allowing insight into these effects; however, much more investigation is required in order to fully understand mismatch effects on the kinetics of ss-DNA molecules. Our initial examination of this process makes clear that the model proposed here is an efficient tool for quantifying the sequence dependent effects of structural transitions. Moreover, the relative simplicity of the model should allow us to study the much larger hairpin structures utilized in recent single-molecule experiments.[1]

V. CONCLUSIONS

In this article, we have presented results obtained from a BD model for simulating ssDNA hairpin loops. The model is able to capture: (i) the effects of temperature on the melting of hairpins, (ii) the kinetics of hairpin formation, and (iii) effects of mismatched sequences in the binding section of the hairpins and opening and closing rates. Although we have not presented a detailed systematic study of all system parameters, we have illustrated the utility of the current model to capture the overall behavior of ssDNA hairpins. On the thermodynamic end, we have seen that more work remains to fine-tune the parameters of our model to provide more robust predictions, especially if the model is expected to produce the realistic dimensional results one obtains with the *m*-fold server. On the kinetic end, we have found that the opening rate is not quenched at low temperatures, which leads to broader distributions in the chain end-to-end probability distribution than one would expect if the hairpin were truly "closed" at low temperatures. We also observed that the melting transition can be attributed to a rapid increase in the opening rate rather than a significant quenching of the closing rate, in agreement with experimental kinetic data.[4] The latter behavior persists when the chain possesses mismatches in the hairpin stem.

We have made occasional comparison between the melting temperatures obtained here and those obtained by the *m*-fold server. In general, we have not found that our model quantitatively captures the default *m*-fold data with the particular parameter values employed in our simulations. We could undertake a brute force approach where we systematically vary our simulation parameters (as well as those on *m*-fold) to search for a regime of the phase space where the melting temperatures agree. Such an agreement would be superficially satisfying, but it is ultimately just a comparison between two different models. Moreover, finding such agreement would only confirm that our model captures a single

metric describing the ssDNA (the melting temperature) rather than the full temperature response. To improve our model, we are presently comparing our simulations with a systematic experimental examination of hairpin melting curves obtained from quencher-emitter end labeled hairpins, for various hairpins and for several different buffers. Not only will this approach provide an unambiguous test of our model but it will also furnish the proportionality constant between the dimensionless temperature employed here and the true system temperature.

This type of model is applicable to hairpins in other situations (for example, in microarrays and in molecular beacon type systems) where one can apply this simulation method to model the dynamics of ssDNA binding to complementary strands. This model can be used to examine specific systems including the binding/unbinding of ssDNA to surface tethered ssDNA and, for example, it can also be used to examine in a systematic manner molecular beaconlike systems. It is also of interest to include the effects of the fluorophores tethered to the ends of the molecule to probe the resulting effects on the dynamics of the ssDNA hairpins. Other possible extensions of this work include examining the effects of hydrodynamic interactions and more detailed models of the electrostatics on the hairpin dynamics.

ACKNOWLEDGMENTS

This work was supported by a Career Development Award from the International Human Frontier Science Program Organization. M.K. would like to thank the University of Minnesota Supercomputing Institute (MSI) for a postdoctoral fellowship. This work was carried out in part using computing resources at the University of Minnesota Supercomputing Institute.

[1] M. T. Woodside, P. C. Anthony, W. M. Behnke-Parks, K. Larizadeh, D. Herschlag, and S. Block, Science **314**, 1001 (2006).
[2] M. T. Woodside, W. M. Behnke-Parks, K. Larizadeh, K. Travers, D. Herschlag, and S. Block, Proc. Natl. Acad. Sci. U.S.A. **103**, 6190 (2006).
[3] W. J. Greenleaf, K. L. Frieda, D. A. N. Forster, M. T. Woodside, and S. M. Block, Science **319**, 630 (2008).
[4] G. Bonnet, O. Krichevsky, and A. Libchaber, Proc. Natl. Acad. Sci. U.S.A. **95**, 8602 (1998).
[5] B. Dubertret, M. Calame, and A. J. Libchaber, Nat. Biotechnol. **19**, 365 (2001).
[6] C. M. Strohsahl, B. L. Miller, and T. D. Krauss, Nature Protocols **2**, 2105 (2007).
[7] S. Tyagi and F. R. Kramer, Nat. Biotechnol. **14**, 303 (1996).
[8] S. Chavali, A. Mahajan, R. Tabassum, S. Maiti, and D. Bharadwaj, Bioinformatics **21**, 3918 (2005).
[9] V. Bloomfield, D. Crothers, and I. Tinoco, Jr., *Nucleic Acids: Structures, Properties, and Functions* (University Science Books, Sausalito, CA, 2000).
[10] M. Zuker, Nucleic Acids Res. **31**, 3406 (2003).
[11] J. Errami, M. Peyrard, and N. Theodorakopoulos, Eur. Phys. J. E **23**, 397 (2007).
[12] M. Wallace, L. Ying, S. Balasubramanian, and D. Klenerman, Proc. Natl. Acad. Sci. U.S.A. **98**, 5584 (2001).
[13] A. Vologodskii and V. Anshelevich, Nucleic Acids Res. **3**, 3377 (1976).
[14] S. M. Bhattacharjee, C. Micheletti, and A. Stasiak, J. Phys.: Condens. Matter **18** (2006).
[15] W. Olson, Curr. Opin. Struct. Biol. **6**, 242 (1996).
[16] S. Harvey, C. Wang, S. Teletchea, and R. Lavery, J. Comput. Chem. **24**, 1 (2003).
[17] T. Knotts IV, N. Rathore, D. Schwartz, and J. de Pablo, J. Chem. Phys. **126**, 084901 (2007).
[18] K. Drukker, G. Wu, and G. Schatz, J. Chem. Phys. **114**, 579 (2001).
[19] M. Sales-Pardo, R. Guimerà, A. Moreira, J. Widom, and L. Amaral, Phys. Rev. E **71**, 051902 (2005).
[20] K. Drukker and G. Schatz, J. Phys. Chem. B **104**, 6108 (2000).
[21] S. Mielke, N. Grønbech-Jensen, V. Krishnan, W. Fink, and C. Benham, J. Chem. Phys. **123**, 124911 (2005).
[22] S. Kannan and M. Zacharias, Biophys. J. **93**, 3218 (2007).
[23] A. Jayaraman, C. Hall, and J. Genzer, Biophys. J. **91**, 2227 (2006).
[24] A. Jayaraman, C. Hall, and J. Genzer, J. Chem. Phys. **127**, 144912 (2007).
[25] H. K. Tsao, J. Z. Y. Chen, and Y. J. Sheng, Macromolecules **36**, 5863 (2003).
[26] E. J. Sorin, Y. M. Rhee, B. J. Nakatani, and V. S. Pande, Biophys. J. **85**, 790 (2003).
[27] S. Buyukdagli, M. Sanrey, and M. Joyeux, Chem. Phys. Lett. **419**, 434 (2005).
[28] N. Bruant, R. Lavery, and D. Genest, Biophys. J. **77**, 2366 (1999).
[29] R. Bird, C. Curtis, R. Armstrong, and O. Hassager, *Dynamics of Polymeric Liquids Volume 2: Kinetic Theory* (Wiley, New York, 1988).
[30] M. P. Allen and D. J. Tildesley, *Computer Simulation of Liquids* (Clarendon, New York, 1987).
[31] R. Jendrejack, J. de Pablo, and M. Graham, J. Chem. Phys. **116**, 7752 (2002).
[32] D. Ermak and J. McCammon, J. Chem. Phys. **69**, 1352 (1978).
[33] Z. Tan and S. Chen, Biophys. J. **95**, 738 (2008).
[34] T. Cheatham III and M. Young, Biopolymers **56**, 232 (2001).
[35] C. Forrey and M. Muthukumar, Biophys. J. **91**, 25 (2006).
[36] I. Teraoka, *Polymer solutions* (Wiley, New York, 2002).
[37] The *m*-fold server does not allow for pairing between the 3′ and 5′ nucleotides. In order to compare the same number of bonded bases, we added on G to each end of the chain used for the *m*-fold server. For example, the hairpin $A_6G_8T_6$ was entered as $GA_6G_8T_6G$. The *m*-fold data were obtained using the DINAMELT program with the two-state melting (folding) option, using the salt concentrations 1*M* Na^+ and no Mg^{+2}.
[38] J. Santa Lucia, Jr., Proc. Natl. Acad. Sci. U.S.A. **95**, 1460 (1998).
[39] J. Hanne, G. Zocchi, N. Voulgarakis, A. Bishop, and K. Rasmussen, Phys. Rev. E **76**, 011909 (2007).
[40] G. Bonnet, S. Tyagi, A. Libchaber, and F. R. Kramer, Proc. Natl. Acad. Sci. U.S.A. **96**, 6171 (1999).
[41] A. Van Orden and J. Jung, Biopolymers **89**, 1 (2008).